NASA Technical Paper 1661

A Scanning Laser-Velocimeter Technique for Measuring Two-Dimensional Wake-Vortex Velocity Distributions

Luther R. Gartrell and David B. Rhodes

MAY 1980

NASA

NASA Technical Paper 1661

A Scanning Laser-Velocimeter Technique for Measuring Two-Dimensional Wake-Vortex Velocity Distributions

Luther R. Gartrell and David B. Rhodes
Langley Research Center
Hampton, Virginia

National Aeronautics
and Space Administration

**Scientific and Technical
Information Office**

1980

SUMMARY

A rapid scanning two-dimensional laser velocimeter (LV) has been used to measure simultaneously the vortex vertical and axial velocity distributions in the Langley Vortex Research Facility. This system utilized a two-dimensional Bragg cell for removing flow-direction ambiguity by translating the optical frequency for each velocity component, which was separated by band-pass filters. A rotational scan mechanism provided an incremental rapid scan to compensate for the large displacement of the vortex with time. The data were processed with a digital counter and an on-line minicomputer. Vaporized kerosene (0.5-μm to 5-μm particle sizes) was used for flow visualization and LV scattering centers. The overall measured mean-velocity uncertainty is less than 2 percent. These measurements were obtained from ensemble averaging of individual realizations.

INTRODUCTION

The laser Doppler velocimeter (LV) has rapidly become an accepted diagnostic tool in the field of fluid dynamics research. There are basically two types (i.e., the reference beam (ref. 1) and the dual scatter or "fringe" system (ref. 2)). The fringe system has been used more extensively because of its superior performance capability and relative ease of application as compared with the reference beam system. It exhibits better signal-to-noise ratios and can be operated either in the backscatter mode or the forward scatter mode. (The geometry of the test environment often dictates the operating mode best suited for a particular measurement situation.) Some of the important features of the LV are as follows:

(1) It is a nonintrusive technique which is less likely to disturb the flow than meaurement devices such as hot-wire probes.

(2) The velocity is measured directly (i.e., independent of other flow parameters such as temperature and pressure), which consequently eliminates the need for complex instrument calibrations or the need for other quantitative parameters.

(3) Good spatial resolution can be obtained for detailed flow-structure studies.

(4) The LV system is highly responsive to local-flow velocity fluctuations in both magnitude and direction.

As the measurement requirements in complex aerodynamic flow have increased, so has the design sophistication of LV instrumentation to comply with these needs. For

instance, during the past several years, vortex research has been expanding rapidly (refs. 3 to 11). Most of this research expansion has been attributed to the advent of the wide-body jet transport for which lift-induced vortices generated by the aircraft present a potential hazard to other encountering aircraft. This phenomenon has led to the need for instrumentation to measure the vortex velocity structures and to obtain quantitative information on the vortex characteristics. A number of methods have been investigated. For example, probes such as hot wires (refs. 12 to 14) and pressure sensors (ref. 15) have been used. These devices, as previously stated, are subject to producing flow disturbances and often require calibration before the data can be interpreted. This is particularly true in more severe test environments where the meandering motion of the vortex system can further complicate the data reduction.

The applications of LV to swirling flows have been documented. Lennert et al. (ref. 16) used a nonscanning LV system for mapping the flow field of wing-tip vortices of a flying aircraft. A scanning LV system, approximately 1 scan/sec and translation speed/scan up to 1.6 m/sec, has been used for measuring vortex velocities in a wind tunnel (ref. 17) and a water towing facility (ref. 18). However, in a static-air towing facility where the vortex drift (downwash) is relatively large and produces transient type measurements, much higher scan rates are needed. To accurately define the vortex velocity distribution in this type facility, scan rates on the order of 30 Hz (scans/sec) were required. This report describes a rapid scanning two-dimensional (i.e., vertical and axial) LV system developed for the Langley Vortex Research Facility and the related systems' tests and evaluations. Typical results of these tests are given.

A discussion of the tracking fidelity of the LV scattering centers (particles) in the vortex flow is presented in the appendix written by Michael J. Walsh.

Use of trade names or names of manufacturers in this report does not constitute an official endorsement of such products or manufacturers, either expressed or implied, by the National Aeronautics and Space Administration.

SYMBOLS

A	aspect ratio
b	model wing span, m
C_D	drag coefficient
C_L	lift coefficient

D	particle diameter, m
D_v	sample volume diameter, m
f_B	effective Bragg cell modulation frequency, MHz
f_c	counter reference clock frequency, MHz
f_d	Doppler frequency, MHz
f_d'	$= f_B \pm f_d$
M	number of threshold crossings
m	exponent
N	total number of individual velocity measurements
$N_{Re,r}$	relative Reynolds number
n	refraction index
r	vortex radius, m
S	distance of apparent shift of focus, m
S_f	fringe spacing, mm
T_r	counter reset time, sec
t	window thickness, mm
u	half-cone angle of laser beam, deg
u_p	angle of laser beam to the normal to the window, deg
V	particle velocity, m/sec
V_{fr}	fringe velocity, m/sec

V_i	individual measured velocity, m/sec
V_∞	model velocity, m/sec
$\overline{V}$	mean velocity, m/sec
$\overline{V}_m$	measured velocity, m/sec
x	distance in direction of center line of vortex, m
y	spanwise distance (coordinate in crossflow plane of vortex), m
y_c	lateral distance of vortex core from plane of symmetry, m
z	coordinate in crossflow plane of vortex
α	angle of attack, deg
β	angle of incidence, deg
β'	angle of refraction, deg
γ	turbulence intensity
θ	angle between intersecting laser beams, deg
λ	laser wavelength, m
μ	viscosity, N-sec/m^2
ρ	density, kg/m^3
σ	standard deviation

Subscripts:

g	gas
p	particle

x	x-component
y	y-component
z	z-component

An arrow over a symbol represents a vector quantity.

VELOCITY MEASUREMENT TECHNIQUE

The velocity measurement technique may be better understood by considering the basic principles of the laser velocimeter, which depends on Mie scattering and the Doppler effect. Shown in figure 1 is a simplified illustration of the fringe model where two parallel coherent beams of radiation of equal intensity are focused by a lens to form "interference fringes" at the focal plane (sample volume). The fringe pattern is in the form of equal light and dark regions. The fringe spacing S_f is given by

$$\frac{\lambda}{2 \sin (\theta/2)} \tag{1}$$

where λ is the wavelength of the laser radiation and θ is the angle between the intersecting beams.

Individual particles (typically several micrometers in diameter) embedded in the moving fluid pass through the fringes, thus causing light to be scattered. This scattered light is detected by a photodetector, thereby generating a fluctuating electrical current in the form of a burst signal at a periodic frequency f_d given by

$$\frac{2 |v| \sin (\theta/2)}{\lambda} \tag{2}$$

where $|v|$ is the absolute normal velocity component of the particle crossing the fringe pattern. The Doppler shift principle can also be used to describe the LV measurement technique (ref. 19), where the frequency of the incident light from each of the beams scattered by the particles in the flow is changed by the movement of particles through the beams. By mixing these frequencies optically, a difference frequency proportional to the velocity of the particle can be detected, thus yielding the same results as shown in equation (2).

Velocity directionality can be obtained with the use of a Bragg cell. This device produces moving fringes, with a velocity proportional to the Bragg cell modulation frequency. The Bragg Doppler-shifted frequency f_d' is given by

$$f_B \pm f_d \tag{3}$$

where f_B is the Bragg cell modulation frequency and f_d is the Doppler frequency. Particles moving in the same direction as the fringes will produce a frequency shift lower than the modulating frequency. The converse is true for particles moving in the opposite direction of the fringes.

Optical System

The optical system used in the present tests (fig. 2) is a confocal system configured to operate in the backscatter mode (i.e., utilizes a common lens arrangement for both transmitting and receiving). It is similar to that of reference 20, with the significant difference being a unique incremental scanning mechanism (ref. 21).

The laser velocimeter uses an argon-ion laser that operates in the TEM_{00} mode and provides up to 5 W of continuous power at the 514.5-nm wavelength. The laser output beam is focused by a 2-diopter lens into the center of a two-dimensional ultrasonic Bragg cell. The Bragg cell allows two orthogonal velocity components (axial and vertical) to be measured. The cell diffracts the incoming laser beam into an array of several diffraction orders. The diffracted orders of the laser beam have the Bragg cell frequencies added to the laser's normal optical frequency. The zero order, (0,0), has only the optical frequency, whereas the diffracted first orders, (0,1) and (1,0), have the optical frequency plus the Bragg cell frequency for that axis. The focusing of the laser beam by the 2-diopter lens minimizes the laser-beam diameter near the origin of the angular divergence of the diffracted orders. This results in a minimum beam diameter for the projected focus in the test section. The Bragg cell is positioned so that the maximum energy is diffracted into the shifted orders. The power to the drivers is then adjusted until the optical power in the (0,0) order, the (0,1) order, and the (1,0) order is equal. The power in the cross order, (1,1), is then also equal. The equalized intensity in the laser beams produces maximum fringe contrast at the projected focus (sample volume). A more elaborate discussion of this procedure is given in reference 22. The Bragg cell is driven at 15 and 25 MHz for the axial and vertical components, respectively. These frequencies were selected so that each velocity component could be retrieved from the photodetector signal by band-pass filters with minimum cross talk. The four orders from the Bragg cell are then collimated by a 1.5-diopter lens, transmitted through a four-hole detector mirror, and imaged into the dead air space of an optical cell by a 20-diopter F1:1.5 lens. The optical cell is used to eliminate extraneous Doppler signals from particles passing through this primary focus. The beams emerging from the optical cell then pass through the scan wheel. This wheel is a 40.5-cm-diameter disk containing 16 windows. The windows vary in thickness from 0 to 30 mm, in 2-mm increments. All windows are

fabricated from schlieren-grade optical crown from the same melt, with both faces parallel to 5 arc sec of wedge or less, flat to 1/10 wave of mercury green light, and antireflection-coated to reduce the effects of aberrations.

The astigmatic and spherical aberrations introduced by the windows can be calculated by knowing the cone angle of the beam, the thickness, and index of refraction of the window (ref. 23). (See sketch (a).)

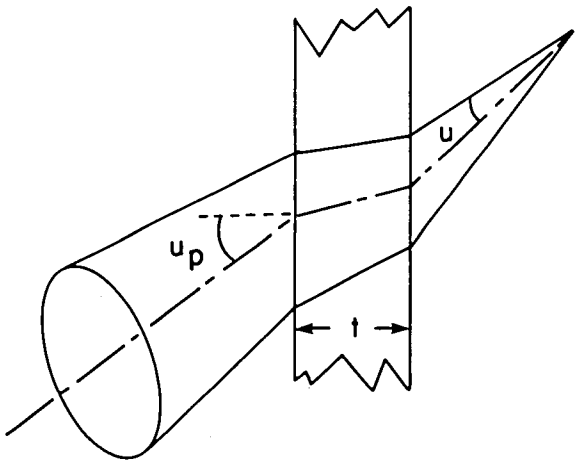

Sketch (a)

The spherical aberration (S.A.) is given by

$$\frac{t}{n}\left(1 - \frac{n \cos u}{\sqrt{n^2 - \sin^2 u}}\right) \tag{4}$$

where u equals half of the cone angle of the beam. For the system discussed herein with a cone angle of approximately 1°, an index of refraction of 1.57, and a window thickness of 30 mm, the spherical aberration is approximately 1.7 μm. The astigmatism is given by

$$\frac{-t}{\sqrt{n^2 - \sin^2 u_p}}\left[\frac{n^2 \cos^2 u_p}{\left(N^2 - \sin^2 u_p\right)} - 1\right] \tag{5}$$

where u_p is the angle of the beam to the normal to the window which is, again, of thickness t and index of refraction n. For this system with the angle of the beam to the normal to the window of approximately 3.5°, the astigmatism is approximately 41.8 μm.

The scan wheel provides scan rates (longitudinal displacement of the focus along the optical axis) up to 30 times/sec, with 16 discrete individual measurement positions for each scan. It operates on the refraction principle, whereby the insertion of plane parallel windows (of various thicknesses) between the primary focus in the optical cell and a projection lens arrangement produces an apparent incremental longitudinal displacement of the primary focus. The displacement due to refraction is shown in sketch (b).

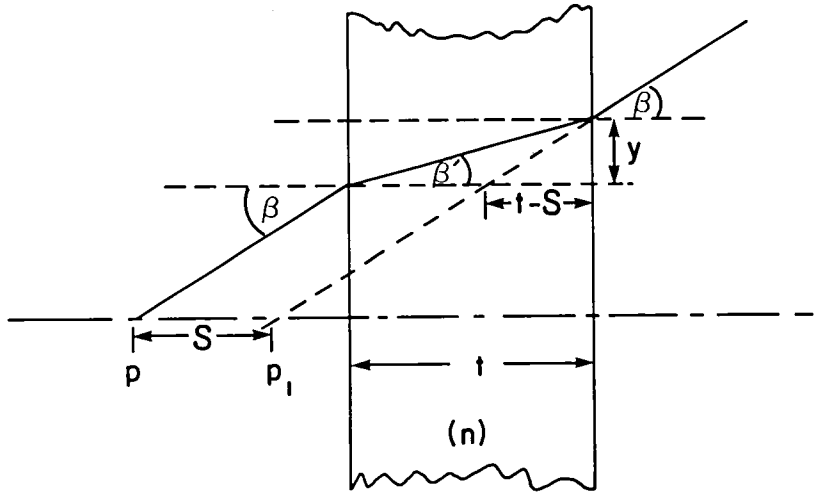

Sketch (b)

If the thickness of the window is t, the refractive index n, the angle of incidence β, and the angle of refraction β', then the displacement S may be shown to be

$$y = t \tan \beta' = (t - S) \tan \beta \tag{6}$$

$$S = t\left(1 - \frac{\tan \beta'}{\tan \beta}\right) \tag{7}$$

and by Snell's law

$$S = \frac{t}{n}\left(n - \frac{\cos \beta}{\cos \beta'}\right) \tag{8}$$

This displacement is magnified (by a factor of approximately 50) by the 2-lens projection system. The first projection lens is a 100-mm-diameter F1: 4 lens corrected to better than $\lambda/8$ wave-front deformation. The second projection lens is an F1: 5.6, with an

effective focal length of 127 cm. The two lenses are separated by about 76.2 cm. This separation can be varied to allow the positioning of the projected LV focus across the test section. The scan range encompassed by the higher speed scan is 0.4 m at a nominal 3-m projected distance. The sample volume formed in the test section is typically 0.2 mm in diameter and 1.4 cm long at the 3-dB level. The actual sensing-sample volume depends on the discrimination level of the processing instrumentation. The sample-volume length given was measured by moving a diffuse scatterer through the sample volume and normalizing the detected output. The sample-volume diameter was measured with a microscope. Particles in the test section crossing the projected focus (sampling volume) scatter light which is collected and imaged back through the lens system and scan wheel to emerge as a collimated beam from the F1: 1.5 lens. The collimated beam is directed by the flat detector mirror to a 190-mm focal-length lens. This lens images the collimated beam onto a 105-μm-diameter pinhole. The light passing through the pinhole is detected by a photomultiplier.

Signal Conditioning Electronics

The signal conditioning electronics shown in figure 3 consist of a photodetection assembly, a digital frequency counter, and a minicomputer plus peripheral equipment.

A high-gain, low-noise photomultiplier with a S-20 wavelength response was used to detect the light scattered by the particles passing through the sample volume and collected by the optical system. The photomultiplier output was coupled to a matching 50-ohm line-driver amplifier.

Band-pass filters (25 MHz and 15 MHz) were used to separate the vertical and axial velocity information transmitted by the Bragg cell carrier frequencies. Mixers were employed to downshift the frequency spectrum for each component by driving them at 20 MHz to produce an effective Bragg frequency of 5 MHz. This was done to reduce the probable operating error of the digital frequency counter.

A simplified diagram of the digital counter-type processor is shown in figure 4. It is a time-domain device which uses a direct counting approach for the time it takes a particle to traverse a preset number of successive fringes. This approach eliminates most of the data ambiguity derived from frequency domain processors such as spectrum broadening effects because of the finite transit time for a particle to pass through the sample volume (ref. 1). Other advantages include the lower input signal-to-noise ratio and duty cycle (Doppler burst rate) required, as opposed to spectrum analyzers and frequency trackers. The input signal, in a form of a Doppler burst, is filtered to remove the pedestal voltage. The resulting signal is applied to a double-threshold zero-crossing detector, a dual-function device used as a wave shaper and noise rejector for reducing the likelihood of false data. A simplified operation of this network is as follows: The first

zero crossing is detected only after the input signal with a positive slope crosses the negative threshold level. In a similar fashion, the second zero crossing is detected when the input signal with a negative slope exceeds the positive threshold level. Continuing this process generates a series of square pulses of constant amplitude. The first two pulses reset and arm the clock-counting circuits. The third pulse starts the period-counting process. Additional noise rejection is achieved with a data validation circuit. It has two identical timing circuits (i.e., a 5- and 8-cycle time count) driven with a 500-MHz reference clock (2-nsec resolution). The output for each circuit is applied to a comparator network. If the resulting 5:8 comparison falls within the preselected limits (0 to 10 percent), the data are accepted as valid.

The validated data go to a storage register which has a binary digital output and is interfaced to a minicomputer. There are 10 data lines and 4 exponent lines for covering a Doppler frequency range of 1.2 kHz to 100 MHz. Additional lines for external inhibit and synchronization are also available. The frequency f_d' is determined from the conversion equation

$$\text{Frequency} = \frac{3.2 \times 10^{10}}{2^m \times \text{reading}}$$

where the values of the exponent m and the reading are indicated by the digital counter processor. These values go into the minicomputer (binary form), which is programmed to calculate the frequency from the conversion equation.

A 4-bit optical encoder mounted on the scan wheel is used to identify each measurement location. The output from this device, along with the output data from the digital counters, is fed into a 16-bit minicomputer which catalogs the related velocity measurements in the flow. The data-acquisition operation of the minicomputer is initiated by a photoelectric trip switch activated by the passage of the strut support for the vortex-generating model. The trip switch is located with the plane of the measurement region. After the switch is activated, the computer remains inhibited until all the output lines from the 4-bit encoder are low (indicating the first measurement location). This time delay is stored in the computer. The total time is calculated from scan speed and delay time and is used to correlate measured velocity with vortex age. The mean velocities and associated standard deviation can be computed, tabulated, and plotted as a function of time or position.

SYSTEM PRECISION

The instrumentation error introduced by the laser velocimeter depends basically on the fringe spacing $f(\lambda,\theta)$ and the measured frequency. The laser is equipped with an

etalon in the cavity space to provide a stable excitation-line width of less than 0.001 cm^{-1}. Therefore the effects of fringe spacing due to the uncertainty of the wavelength λ is extremely small and is therefore neglected. The cross-beam angle θ for each measurement location was determined within 0.007°. The velocity bias error due to cross-beam angle is expressed as

$$\frac{\Delta V(\theta)}{V(\theta)} = \left|0.5 \cot (\theta/2)\, \Delta\theta\right| \tag{9}$$

A typical cross-beam angle range from $\theta = 1^{\circ}$ to 0.5° and $\Delta\theta = 1.15 \times 10^{-4}$ rad yields a velocity error of approximately 1 percent.

The velocity error associated with the frequency determination arose from the signal-processing electronics. The error contributed by the signal-processing electronics (digital counters) depends on the quality of the input signal and the internal control parameters of the counter (refs. 24 and 25). For the measurements presented herein, the signal level was generally better than 15 dB above the noise. This level was sufficient to set the counter threshold for discriminating against the noise background.

The main internal control parameters of the counter that affect the system precision are digital quantization and clock synchronization. The following assumptions and procedures outlined in reference 25 are used to approximate the bias and random error contributed by this device. Digital quantizing error (random) occurs during the measurement of the particle transit time (which consists of discrete clock pulses) through a given number of fringes. The synchronization error (bias) develops during the start of the timing sequence where the reference clock frequency and the signal frequency are matched. These error sources in the measured Doppler frequency f_d can be expressed as follows:

Quantization error –

$$\frac{\overline{V}_m(f) - \overline{V}(f)}{\overline{V}(f)} = \pm\frac{q^2}{3}\left(1 + 3\zeta^2\right) \tag{10}$$

where

$$\zeta = \frac{\gamma}{1 + \frac{f_B}{\overline{f}_d}} \tag{11}$$

and

$$q = \frac{f_d'}{Mf_c} \tag{12}$$

Clock synchronization error –

$$\frac{\overline{V}_m(f) - \overline{V}(f)}{\overline{V}(f)} = \frac{q}{2}\left(1 + \zeta^2\right) \tag{13}$$

Terms in equations (10) to (13) are: $\bar{f}_d$, true mean Doppler frequency; f_B, effective Bragg cell frequency; f_c, counter reference-clock frequency; M, number of input signal cycles used for processing; γ, flow turbulence intensity; $\overline{V}_m$, measured velocity; and $\overline{V}$, true velocity. Based on the previous equations, as well as an average Doppler frequency of 0.5 MHz, and effective Bragg cell frequency of 5 MHz, 20-percent flow turbulence intensity, 8-input signal cycles, and 500-MHz reference clock frequency, estimates of these errors are made and summarized in the following table:

Source	Bias, percent	Random, percent
Cross-beam angle	±1.0	----------
Quantization	------	Negligible (<<0.01)
Clock synchronization	.0687	----------

APPLICATION TO VORTEX FLOW FIELD

In order to evaluate the system performance in a swirling flow environment, tests were conducted in the Langley Vortex Research Facility. A schematic diagram of this facility is shown in figure 5. This facility uses a gasoline-powered carriage to tow aircraft models through a static-air test area at a constant velocity. The overhead track for the carriage is 549 m long. The test area is covered (except a 5-cm opening for the model support) to provide isolation of the test-model-generated vortices from the wake of the carriage. The test section is 91.37 m long, 5.49 m wide, and 5.18 m high. For a more detailed description of this facility, see reference 8. The test model (fig. 6) used for generating the wake vortices is a 0.03-scale model of the Boeing 747. It has a wing span of 1.79 m and is equipped with leading- and trailing-edge flaps to simulate a landing or cruise configuration.

The seeding material used in these tests was vaporized kerosene, which has a mass density of 0.82 g/m^3 and a size distribution of 0.5 μm to 5 μm, as shown in figure 7. The size distribution was determined with a commercial particle-sizing system.

The following test procedure was used to obtain a velocity profile measurement of the wake vortex. The vortex-generating model is towed through the test section at a constant nominal velocity of approximately 30 m/sec. (See fig. 8.) As the generated vortex system drifts through the scan region at a nearly constant rate, it is rapidly scanned (30 times/sec) over a distance of approximately 0.4 m. The rapid scan is needed because of the time dependency of the vortex characteristics. Measurements were made in regions covering approximately 1 semispan. Although velocity measurements were made for the entire run time, only vortex core penetrations are presented. Typical measurements at any location during a run were based on approximately 20 velocity determinations during a 2.0-msec observation time. The separation distance of the model from the vortex measuring region was varied by changing the height of the model and keeping the height of the sample regions constant (2.3 m). The model heights above the sample regions were preselected for the purpose of obtaining measurements in the near field (roll-up region) and the far field (along the stable region). These tests were conducted with the model at representative lift coefficients corresponding to the model test configuration. For instance, tests for the landing (flaps) and the cruise (basic aircraft) configurations were with lift coefficients of 1.2 and 0.67, respectively. At the test location, heated kerosene vapor was deployed for flow-field visualization (fig. 9) and LV scattering centers. The resulting flow-visualization data as a function of time are recorded on videotape. A video timer (also initiated by the photoelectric switch) was used for the time display. These measurements complemented the LV measurement by pinpointing the time that the vortex core penetrated the sample region, whereby the corresponding scan number could be determined. Using this technique greatly reduced the data search time.

VELOCITY MEASUREMENT ACCURACY

The operating principle of the LV technique depends partly on Mie scattering and involves measuring the velocity of particles suspended in the moving fluid in order to obtain the velocity of the fluid. In determining the overall measurement accuracy based on this concept, consideration must be given to the particle-flow tracking fidelity. An analysis of particle dynamics in a swirling or vortex flow is discussed in the appendix. It was found that particles (<1 μm) in the vortex core migrate in the radial direction, which results in the lack of data for far-field velocity measurement in the core region. The resulting conclusions of this analysis imply that less than 1-percent error is introduced in the final measurement due to particle-tracking error. Therefore the overall uncertainty in the measured mean velocity, including particle tracking, cross-beam angle measurements, and frequency determination errors, is less than 2 percent.

The measurement data from the digital counters represent the detection of the occurrence of individual events in the flow, whereby the final velocity measurement result is based on an arithmetic ensemble averages. A given set of these individual realizations is expressed as

$$\overline{V} = \frac{1}{N} \sum_{i=1}^{N} V_i \tag{14}$$

$$\sigma = \sqrt{\sum_{i=1}^{N} \frac{(V_i - \overline{V})^2}{N - 1}} \tag{15}$$

with the statistical uncertainty in the mean given as $\pm \frac{\sigma}{\sqrt{N}}$. Data acquired by means of individual realizations, which are subject to biasing effects (i.e., randomly occurring velocity-dependent events in an assumed uniformly seeded flow) will cause the resulting velocity measurement to be biased toward the higher velocities. On the other hand, in flow situations where Bragg cells are used, the velocity measurement is biased toward the lower velocities. Thus, the combined effect has a tendency to reduce the overall bias. There are many proposed treatments for the velocity biasing problem (refs. 26 to 30). McLaughlin and Tiederman (ref. 26) have shown that the corrected velocity (unbiased) can be obtained from weighted ensemble averages, as shown in equation (16)

$$\overline{V} = \frac{1}{N} \frac{\sum_{i=1}^{N} W_i V_i}{\sum_{i=1}^{N} W_i} \tag{16}$$

where the weighting function W_i is expressed as $1/|V|$. Meyers' equation (ref. 27), which takes into account the Bragg frequency, is given by

$$V = \frac{\sum_{i=1}^{N} W_i V_i}{\sum_{i=1}^{N} W_i} \tag{17}$$

where

$$W_i = \frac{10\ S_f + T_r\left(V_{fr} + V_i\right)}{D_v\left(V_{fr} + V_i\right)} \tag{18}$$

S_f fringe spacing

T_r counter reset time

V_i measured velocity

V_{fr} velocity of fringes

D_v sample volume diameter

Corrected velocity data were computed based on equation (17), which takes into account the effects of the Bragg cell. These calculated values were compared with the arithmetic ensemble averages, and the results revealed insignificant differences. Therefore the data presented in this report are derived from arithmetic ensemble averages.

RESULTS AND DISCUSSION

Wake-vortex flow velocity profile measurements were made at a model speed of 30 m/sec. Plots for the cruise and landing configurations are shown in figures 10 and 11, respectively. The measured vortex velocity distribution for the cruise condition was obtained for a 0.67 lift coefficient and separation distance (between the model and the measurement plane) of 7.1 spans. In a similar fashion, measurements were made for the landing configuration, where the lift coefficient is 1.2 and the separation distance is 55 spans. The lack of data points in the vortex core is due to the absence of sufficient scattering centers in this region. Particles are centrifuged out of the core as the flow develops, with the larger particles (>2 μm) migrating out first. For the cruise condition, the vortex drift (downwash) was low enough that several successive scans for the same run could be used for mapping the velocity distribution for essentially the same spatial location. However, for the landing condition where the vortex displacement with time was much larger, separate runs were required. The theoretical curve, superimposed on the measured values, is based on the equation given in reference 31 as

$$\frac{V}{V_\infty} = \frac{C_L}{\pi^2 A}\left[\frac{y - y_c}{|y - y_c|}\left(\frac{6b}{|y - y_c|} - 9\right)^{1/2} + \frac{b}{y - y_c}\right] \tag{19}$$

where C_L is the lift coefficient, A is the aspect ratio, b is the model span, y is the spanwise distance, and y_c is the lateral distance of the vortex core from the plane of symmetry. This equation is the same as used in reference 31 to analyze data obtained with a similar model in a towing basin, and the measured velocity data were in good agreement with the theoretical values over the region compared.

During the simulated landing configuration, several vortices were shed from each wing of the test model. The near-field ($x/b \approx 1$) vertical velocity distribution of the dominant vortex, produced by the outboard flaps, is shown in figure 12. Typical vortex vertical velocity distributions are shown in figure 13 at various separation distances between the model and the measurement region for the basic aircraft. These measurements were made at a nominal lift coefficient of 0.67. The simultaneously measured vertical and horizontal velocity distributions of the wake-vortex system are shown in figure 14. These values are normalized to the model velocity. The peak velocities for the vertical and horizontal velocity components are approximately 25 and 10 percent of the model velocity, respectively. The statistical uncertainty of the mean $\frac{\sigma}{\sqrt{N}}$ for both velocity distributions, when normalized to the model velocity, occurred within the plotting symbols.

CONCLUSIONS

A rapid scanning two-dimensional laser velocimeter (LV) system has been developed and tested in the Langley Vortex Research Facility. On the basis of the results obtained, the following significant observations can be made:

1. The major instrumentation error source was the determination of the cross-beam angles, θ_i, which contributed approximately 1-percent bias error to the system; radiation wavelength and electronic counter contributions were negligible.

2. The overall measurement accuracy involving particle dynamics, measurement statistics, and velocity bias for particles with size distributions of 1 to 3 μm and a specific gravity of 0.82 g/cm^3 contributed less than 1-percent error due to flow tracking fidelity; and the data treatment using ensemble averages with the application of Bragg cells did not require data correction due to velocity biasing effect.

3. The LV system is capable of simultaneously measuring both vertical and axial flow velocity components in a near field or far field of the vortex system, whereby quantitative information can be retrieved.

4. Particles (>1 μm) in the vortex core migrate in the radial direction which results in the lack of data for far-field velocity measurement in the core region.

5. The rapid scan rate minimized the effects of the vortex relative high-drift rate (downwash) so that an accurate definition of the vortex system could be obtained.

6. The measured velocity data were in good agreement with the theoretical calculated values over the region compared.

Langley Research Center
National Aeronautics and Space Administration
Hampton, VA 23665
March 19, 1980

APPENDIX

PARTICLE MOTION IN A VORTEX

Michael J. Walsh
NASA Langley Research Center

The following section analyzes the three-dimensional motion of various size particles passing through a vortex in air.

The general governing equation given by Soo (ref. 32) for a particle traveling in air reduces to the following equation for the special case of a spherical particle traveling in air:

$$\frac{d\vec{V}_p}{dt} = \frac{3}{4}\frac{C_D N_{Re,r}\,\mu_g}{\rho_p D_p^2}\left(\vec{V}_g - \vec{V}_p\right) \tag{A1}$$

where the relative Reynolds number $N_{Re,r}$ is defined as

$$N_{Re,r} = \frac{\rho_g\left|\vec{V}_g - \vec{V}_p\right| D_p}{\mu_g} \tag{A2}$$

Equation (A1) assumes that viscous drag is the only force acting on the particle. As discussed in reference 33, equation (A1) can be treated in component form as

$$\frac{dV_{p,x}}{dt} = \frac{3}{4}\frac{C_D N_{Re,r}\,\mu_g\left(V_{g,x} - V_{p,x}\right)}{\rho_p D_p^2} \tag{A3}$$

$$\frac{dV_{p,y}}{dt} = \frac{3}{4}\frac{C_D N_{Re,r}\,\mu_g\left(V_{g,y} - V_{p,y}\right)}{\rho_p D_p^2} \tag{A4}$$

$$\frac{dV_{p,z}}{dt} = \frac{3}{4}\frac{C_D N_{Re,r}\,\mu_g\left(V_{g,z} - V_{p,z}\right)}{\rho_p D_p^2} \tag{A5}$$

For the present analysis, x is in the direction of the vortex axis, and y and z are in the cross-flow plane of the vortex. To complete the system of six differential equations

that are needed to solve for the three-dimensional particle motion, three additional equations are obtained from the definition of velocity

$$\frac{dx}{dt} = V_{p,x} \tag{A6}$$

$$\frac{dy}{dt} = V_{p,y} \tag{A7}$$

$$\frac{dz}{dt} = V_{p,z} \tag{A8}$$

Thus, the three-dimensional particle motion through a vortex can be computed by a numerical procedure using the gas flow-field velocity V_g, viscosity μ_g, density ρ_g, particle density ρ_p and size D_p, the drag coefficient C_D, and the initial conditions of particle position and velocity. For the present calculations, the gas velocity distribution in the cross-flow plane of the vortex is the theoretical one shown in figure 11 as a function of radial position from the center of the vortex. The velocity component parallel to the vortex axis is equal to 30.9 m/sec. The gas density and viscosity were evaluated at atmospheric pressure and a temperature of 300 K. The particle density was equal to 919.5 kg/m^3. The drag coefficient was evaluated from the following equation given in reference 34:

$$C_D = \frac{24}{N_{Re,r}}\left(1 + 0.15N_{Re,r}^{0.687}\right) \tag{A9}$$

which gives good predictions of incompressible sphere drag for $N_{Re,r} < 200$. For the present calculations, the particles were initially at zero velocity prior to being accelerated by the vortex at $x/b = 0$. The calculations indicated that velocity lags were small (generally less than 1 percent for 1- to 3-μm particles, even though the particles migrate in the radial direction. This means that accurate laser velocimeter (LV) measurements can be obtained with 1- to 3-μm particles.

As previously mentioned, the 1- to 3-μm particles do migrate in the radial direction. It is of interest to see if the particle-motion calculations explain the lack of LV data for $r/b < 0.02$ at $x/b = 55$, which is the measurement station for the LV data presented in figure 11. Changes in the particle's radial distance from the center of the vortex are presented in figure 15 for various size particles passing through the vortex. The data indicate that the change in radial position depends on the particle size and initial radius at $x/b = 0.0$. The dashed line in figure 15 represents the minimum r/b at

which LV measurements could generally be obtained during the present tests. Note that the data in figure 15 are limited to $x/b < 6$ because the calculations were too time-consuming to continue them all the way to $x/b = 55$. It was believed that enough information could be obtained by extrapolating the r/b values for $x/b < 6$ to $x/b = 55$. The calculations indicated that all the particles greater than 2 μm migrate out of the region $r/b < 0.02$ by $x/b = 55$. The only particles left in the region $r/b < 0.02$ at $x/b = 55$ are 1 μm or smaller than were originally at $r/b < 0.01$. This represents a reduction of a factor of 4 in the number density of 1-μm particles for $r/b < 0.02$. Thus, the particle-motion calculations confirm the results obtained in the LV measurements.

REFERENCES

1. Edwards, Robert V.; Angus, John C.; French, Michael J.; and Dunning, John, W., Jr.: Spectral Analysis of the Signal From the Laser Doppler Flowmeter: Time-Independent Systems. J. Appl. Phys., vol. 42, no. 2, Feb. 1971, pp. 837-850.

2. Brayton, D. B.; and Goethert, W. H.: A New Dual-Scatter Laser Doppler-Shift Velocity Measuring Technique. ISA Trans., vol. 10, no. 1, 1971, pp. 40-50.

3. Patterson, James C., Jr.; and Jordan, Frank L., Jr.: A Static-Air Flow Visualization Method To Obtain a Time History of the Lift-Induced Vortex and Circulation. NASA TM X-72769, 1975.

4. Ciffone, D. L.; and Lonzo, C., Jr.: Flow Visualization of Vortex Interactions in Multiple Vortex Wakes Behind Aircraft. NASA TM X-62459, 1975.

5. Garodz, Leo J.; Lawrence, David; and Miller, Nelson: The Measurement of the Boeing 727 Trailing Vortex System Using the Tower Fly-By Technique. Rep. No. FAA-RD-74-90, Aug. 1974. (Available from DTIC as AD 786 569.)

6. Patterson, James C., Jr.; and Jordan, Frank L., Jr.: An Investigation of the Increase in Vortex Induced Rolling Moment Associated With Landing Gear Wake. NASA TM X-72786, 1975.

7. Smith, Harriet J.: A Flight Test Investigation of the Rolling Moments Induced on a T-37B Airplane in the Wake of a B-747 Airplane. NASA TM X-56031, 1975.

8. Patterson, James C., Jr.: Vortex Attenuation Obtained in the Langley Vortex Research Facility. J. Aircr., vol. 12, no. 9, Sept. 1975, pp. 745-749.

9. Croom, Delwin R.: Wind-Tunnel and Flight Evaluation of Spoilers as Trailing-Vortex Hazard Alleviation Devices. AIAA Paper 77-10, Jan. 1977.

10. Rossow, Vernon J.: Convective Merging of Vortex Cores in Lift-Generated Wakes. J. Aircr., vol. 14, no. 3, Mar. 1977, pp. 283-290.

11. Bilanin, Alan J.; Teske, Milton E.; and Williamson, Guy R.: Vortex Interactions and Decay in Aircraft Wakes. AIAA J., vol. 15, no. 2, Feb. 1977, pp. 250-260.

12. Chigier, N. A.; and Corsiglia, V. R.: Tip Vortices – Velocity Distributions. NASA TM X-62087, 1971.

13. Chigier, N. A.; and Corsiglia, V. R.: Wind-Tunnel Studies of Wing Wake Turbulence. J. Aircr., vol. 9, no. 12, Dec. 1972, pp. 820-825.

14. Corsiglia, V. R.; Schwind, R. G.; and Chigier, N. A.: Rapid Scanning, Three-Dimensional Hot-Wire Anemometer Surveys of Wing-Tip Vortices. J. Aircr., vol. 10, no. 12, Dec. 1973, pp. 752-757.

15. Mason, W. H.; and Marchman, J. F., III: Farfield Structure of an Aircraft Trailing Vortex, Including Effects of Mass Injection. NASA CR-62,078, 1972.

16. Lennert, A. E.; Crosswy, F. L.; and Kalb, H. T.: Application of the Laser Velocimeter for Trailing Vortex Measurements. AEDC-TR-74-26, U.S. Air Force, Dec. 1974.

17. Orloff, Kenneth L.; and Grant, George R.: The Application of Laser Doppler Velocimetry to Trailing Vortex Definition and Alleviation. NASA TM X-62243, 1973.

18. Orloff, K. L.; Ciffone, D. L.; and Lorincz, D.: Airfoil Wake Vortex Characteristics in the Far Field. NASA TM X-62318, 1973.

19. Lading, L.: Differential Doppler Heterodyning Technique. Appl. Opt., vol. 10, no. 8, Aug. 1971, pp. 1943-1949.

20. Farmer, W. M.; and Hornhkohl, J. O.: Two-Component, Self-Aligning Laser Vector Velocimeter. Appl. Opt., vol. 12, no. 11, Nov. 1973, pp. 2636-2640.

21. Rhodes, David B.: Optical Scanner. U.S. Pat. 4,063,814, Dec. 20, 1977.

22. Chu, W. P.; and Mauldin, L. E.: Bragg Diffraction of Light by Two Orthogonal Ultrasonic Waves in Water. Appl. Phys. Lett., vol. 22, no. 11, June 1, 1973, pp. 557-559.

23. Smith, W. J.: Modern Optical Engineering – The Design of Optical Systems. McGraw Hill Book Co., Inc., c.1966.

24. Hösel, W.; and Rodi, W.: Errors Occurring in LDA-Measurements With Counter Signal Processing. The Accuracy of Flow Measurements by Laser Doppler Methods, Proc. LDA-Symposium (Copenhagen), 1976, pp. 251-257.

25. Wang, J. C. F.: Measurement Accuracy of Flow Velocity via a Digital-Frequency-Counter Laser Velocimeter Processor. The Accuracy of Flow Measurements by Laser Doppler Methods, Proc. LDA-Symposium (Copenhagen), 1976, pp. 151-175.

26. McLaughlin, D. K.; and Tiederman, W. G.: Biasing Correction for Individual Realization of Laser Anemometer Measurements in Turbulent Flows. Phys. Fluids, vol. 16, no. 12, Dec. 1973, pp. 2082-2088.

27. Meyers, James F.; and Clemmons, James I., Jr.: Processing Laser Velocimeter High-Speed Burst Counter Data. NASA paper presented at 3rd International Workshop on Laser Velocimetry (Lafayette, Indiana), July 1978.

28. Kreid, Dennis K.: Laser-Doppler Velocimeter Measurements in Nonuniform Flow: Error Estimates. Appl. Opt., vol. 13, no. 8, Aug. 1974, pp. 1872-1881.

29. Buchhave, P.: Biasing Errors in Individual Particle Measurements With the LDA-Counter Signal Processor. The Accuracy of Flow Measurements by Laser Doppler Methods, Proc. LDA-Symposium (Copenhagen), 1976, pp. 258-278.

30. Quigley, M. Scott; and Tiederman, William G., Jr.: Experimental Evaluation of Sampling Bias in Individual Realization Laser Aneometry. AIAA J., vol. 15, no. 2, Feb. 1977, pp. 266-268.

31. Kirkman, Karl L.; Brown, Clinton E.; and Goodman, Alex: Evaluation of Effectiveness of Various Devices for Attenuation of Trailing Vortices Based on Model Tests in a Large Towing Basin. NASA CR-2202, 1973.

32. Soo, S. L.: Fluid Dynamics of Multiphase Systems. Blaisdell Publ. Co., c.1967.

33. Cuddihy, William F.; Beckwith, Ivan E.; and Schroeder, Lyle C. (Appendix A by Ivan E. Beckwith, Dennis M. Bushnell, and James L. Hunt; Appendix B by Ivan E. Beckwith and Sadie P. Livingston; and Appendix C by Ivan E. Beckwith): Flight Test and Analysis of a Method for Reducing Radio Attenuation During Hypersonic Flight. NASA TM X-1331, 1967.

34. Torobin, L. B.; and Gauvin, W. H.: Fundamental Aspects of Solids-Gas Flow. Can. J. Chem. Eng., vol. 37, no. 4, Aug. 1959, pp. 129-141.

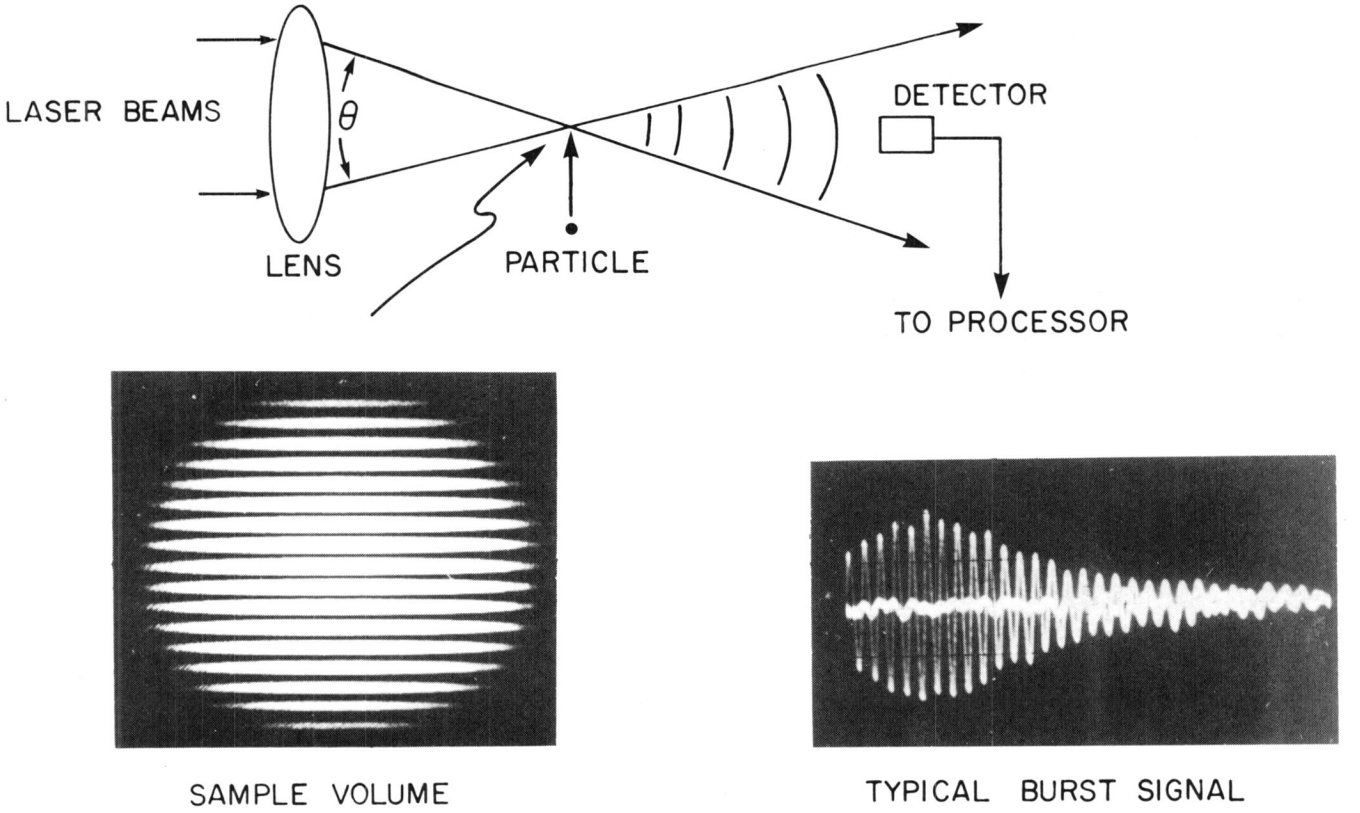

Figure 1.- Laser velocimeter technique.

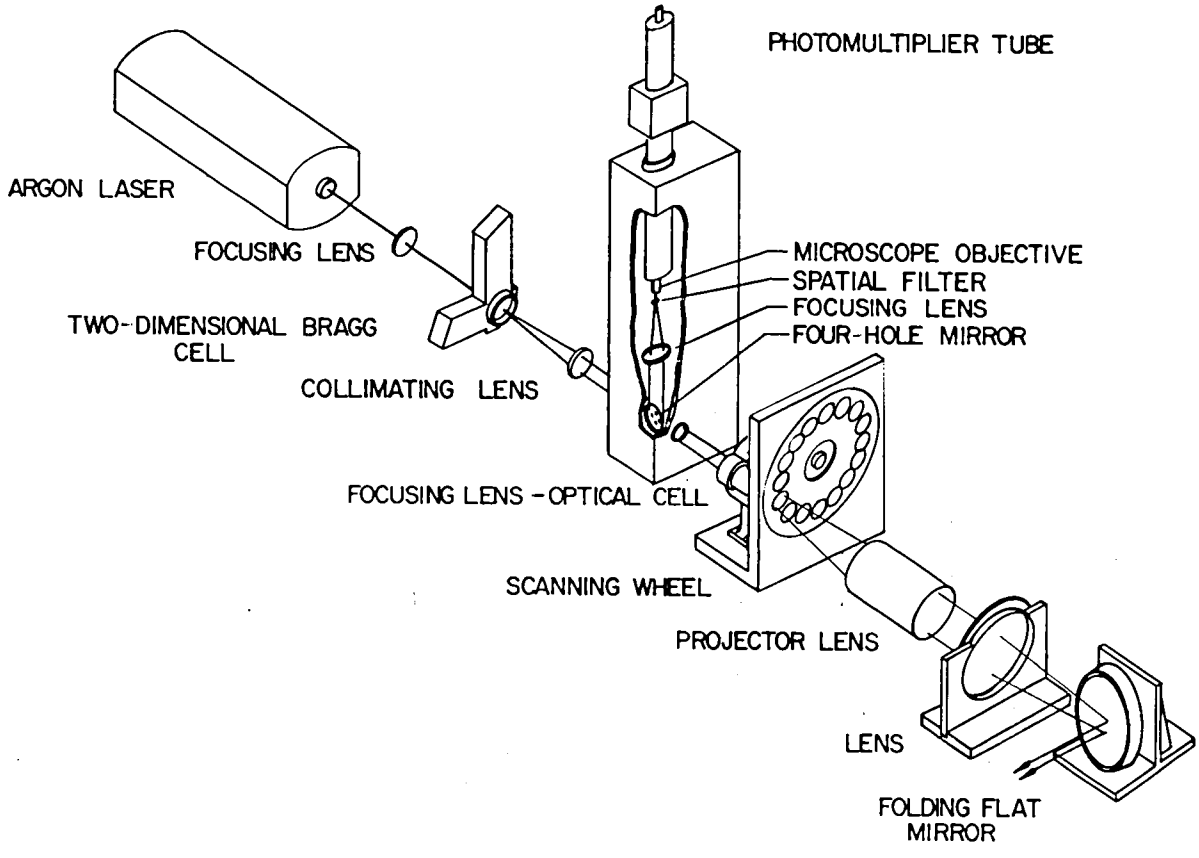

Figure 2.- Optical system.

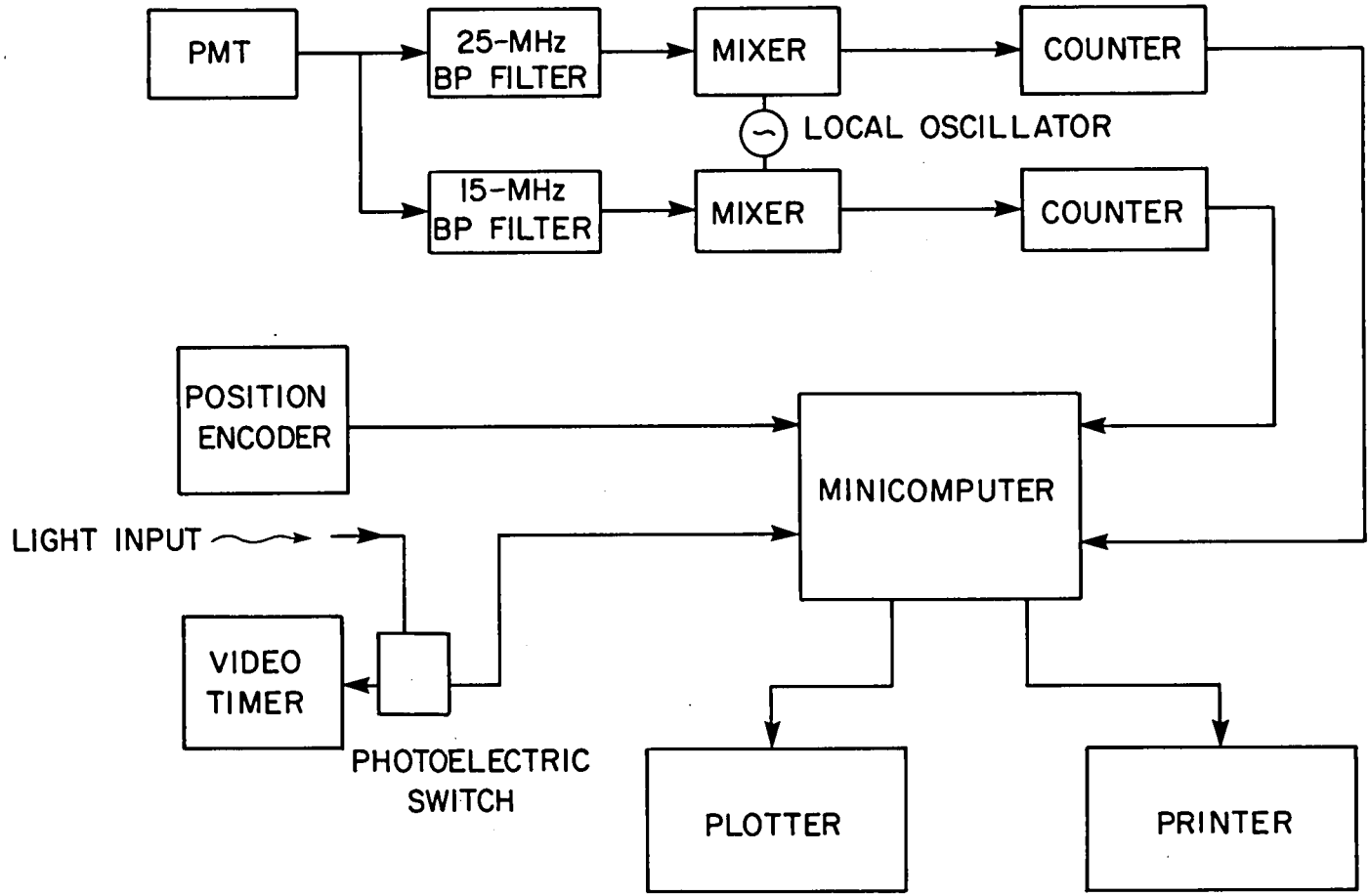

Figure 3.- Data acquisition and processing system. (PMT is photomultiplier tube and BP is band pass).

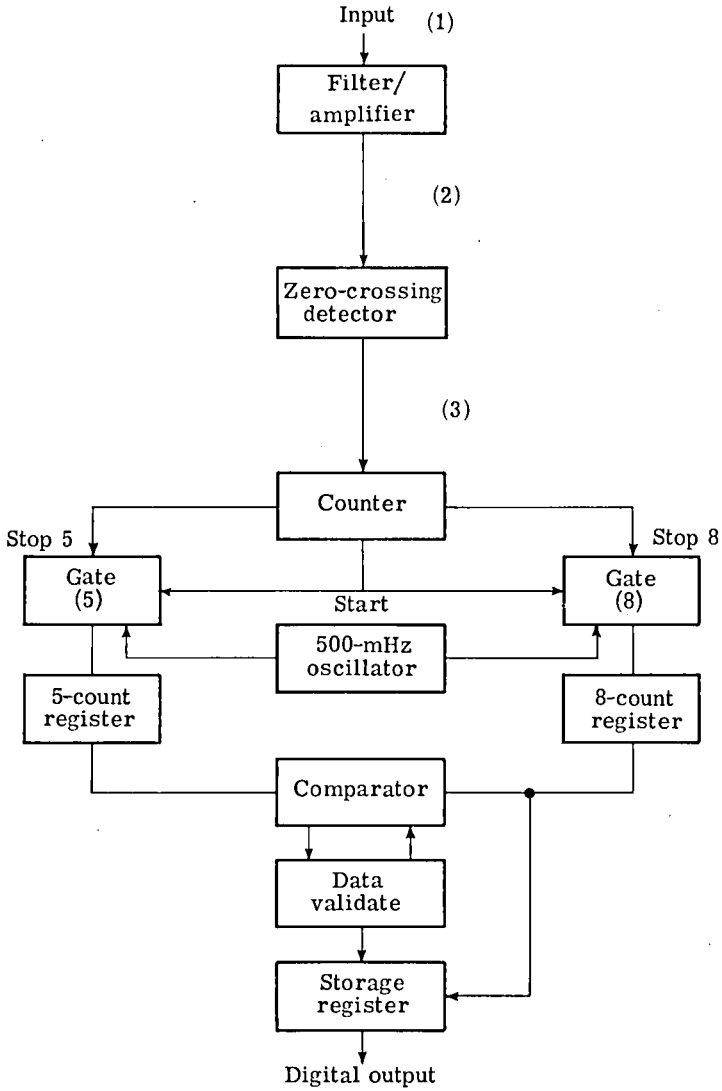

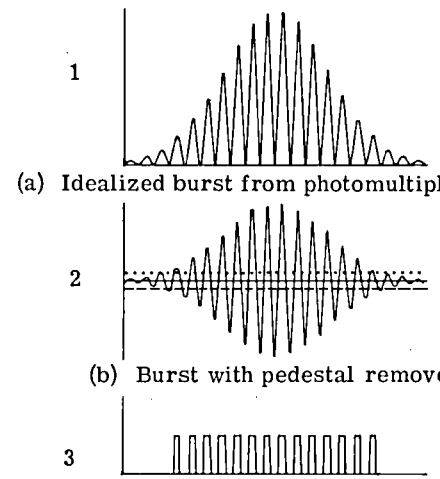

(a) Idealized burst from photomultiplier tube.

(b) Burst with pedestal removed.

(c) Digital pulse train from zero-crossing detector.

Figure 4.- Digital counter-type processor.

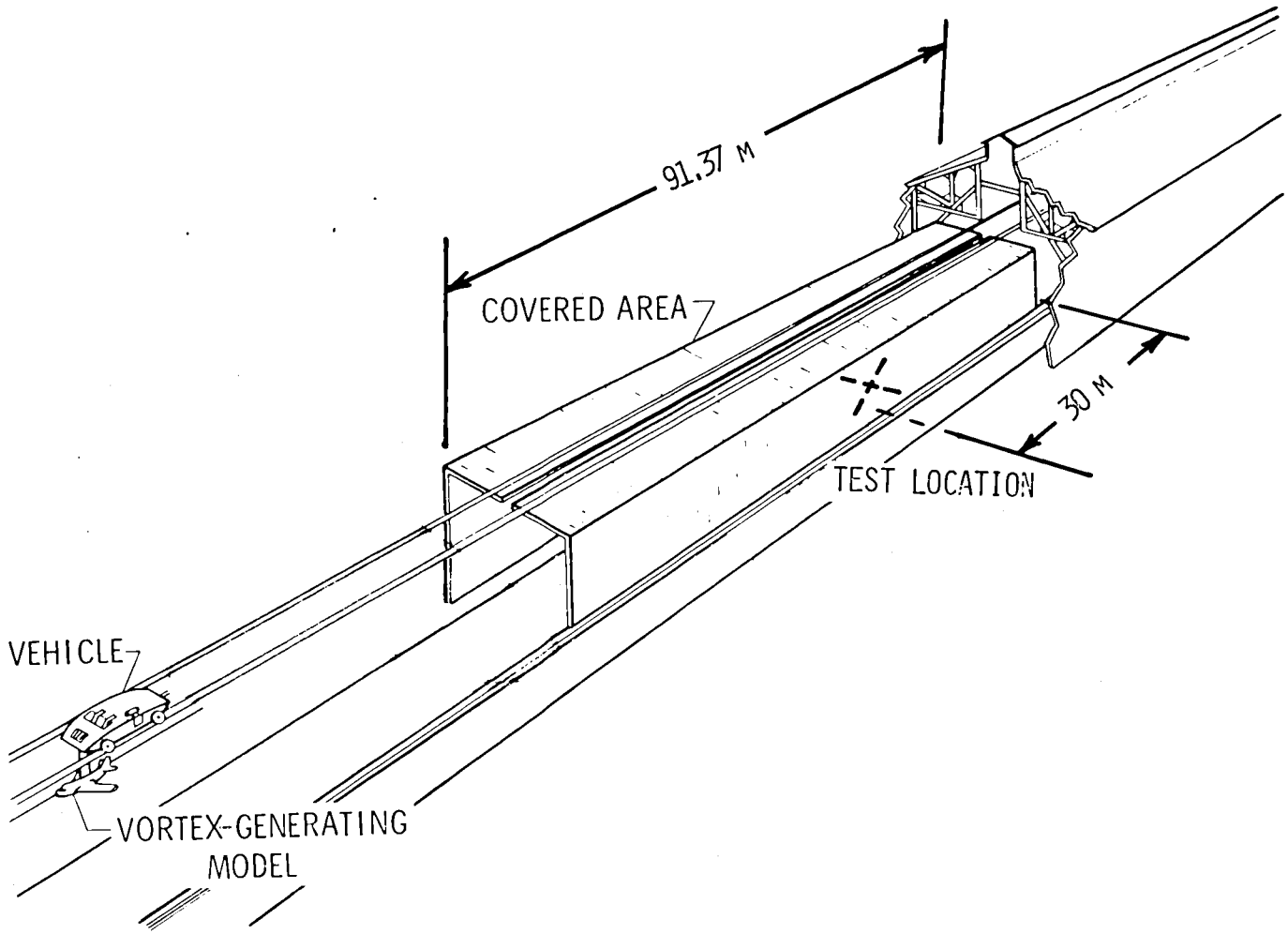

Figure 5.- Langley Vortex Research Facility.

L-76-4044

Figure 6.- The 0.03-scale model.

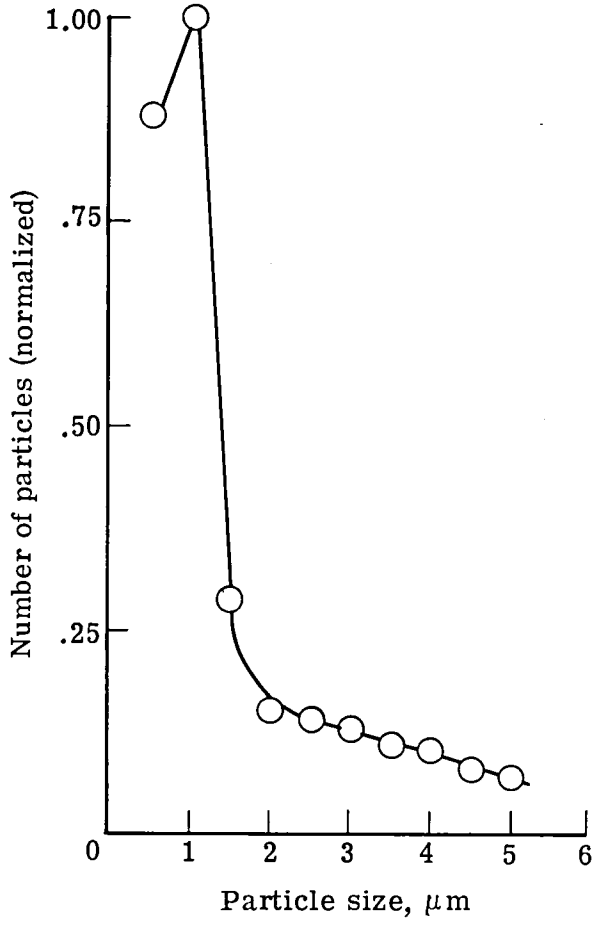

Figure 7.- Size distribution of seeding material.

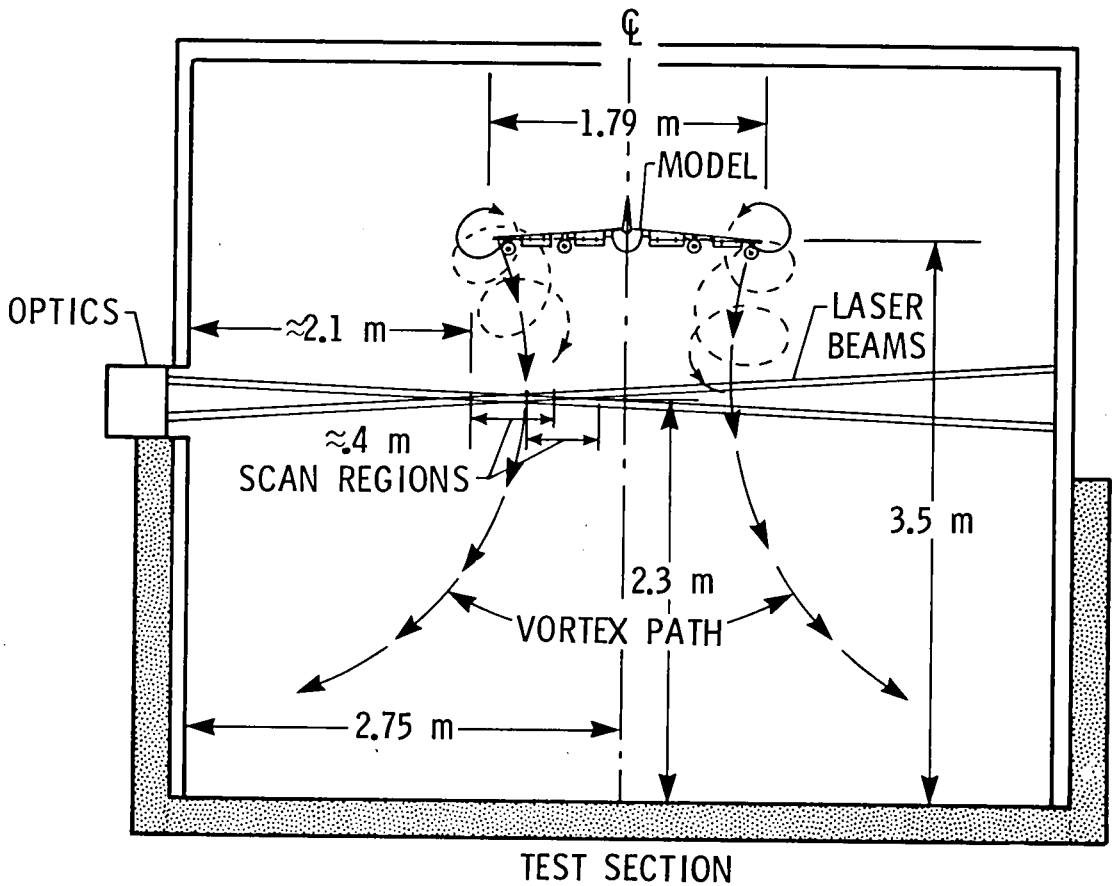

Figure 8.- General scheme for measuring vortex velocity distribution.

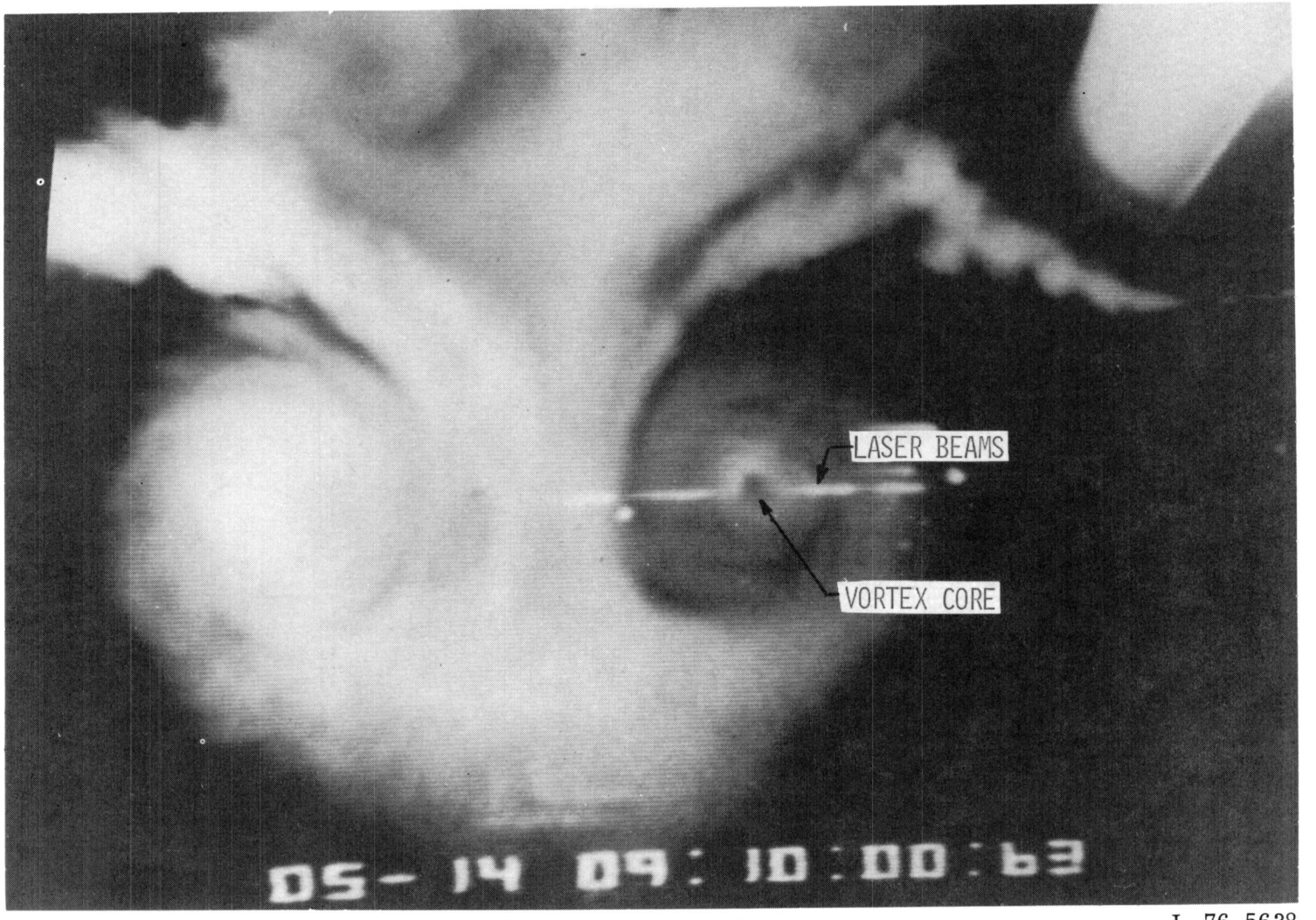

L-76-5638

Figure 9.- Flow visualization of vortex system.

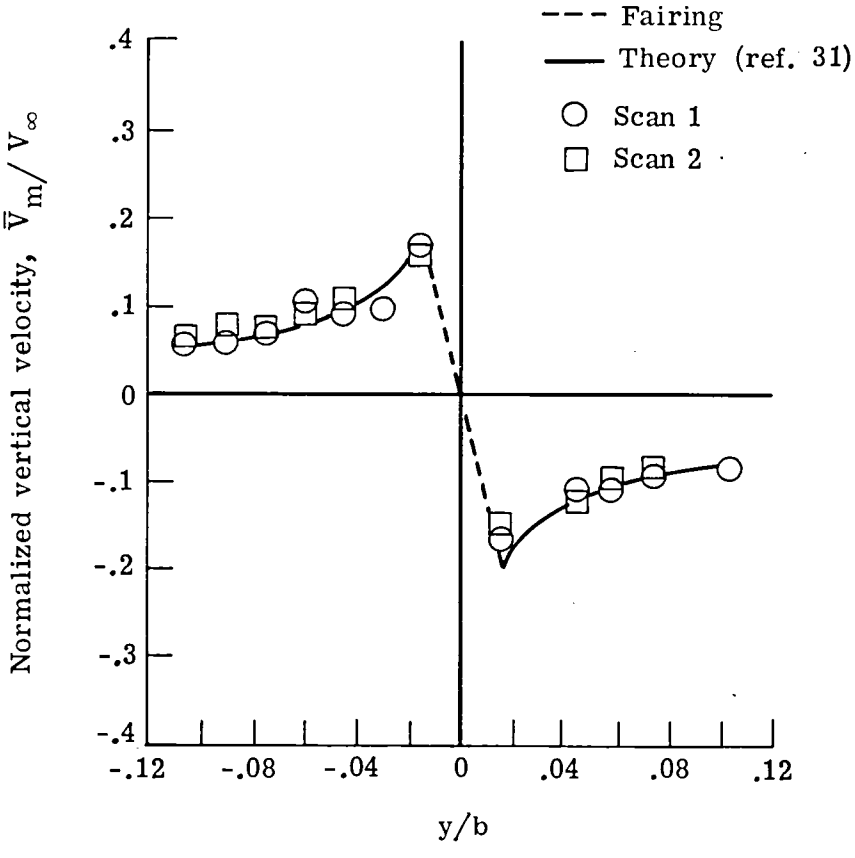

Figure 10.- Vertical velocity distribution at $x/b = 7.1$, $\alpha = 6.33^{o}$, $C_L = 0.65$, and $V_\infty = 30$ m/sec (cruise configuration).

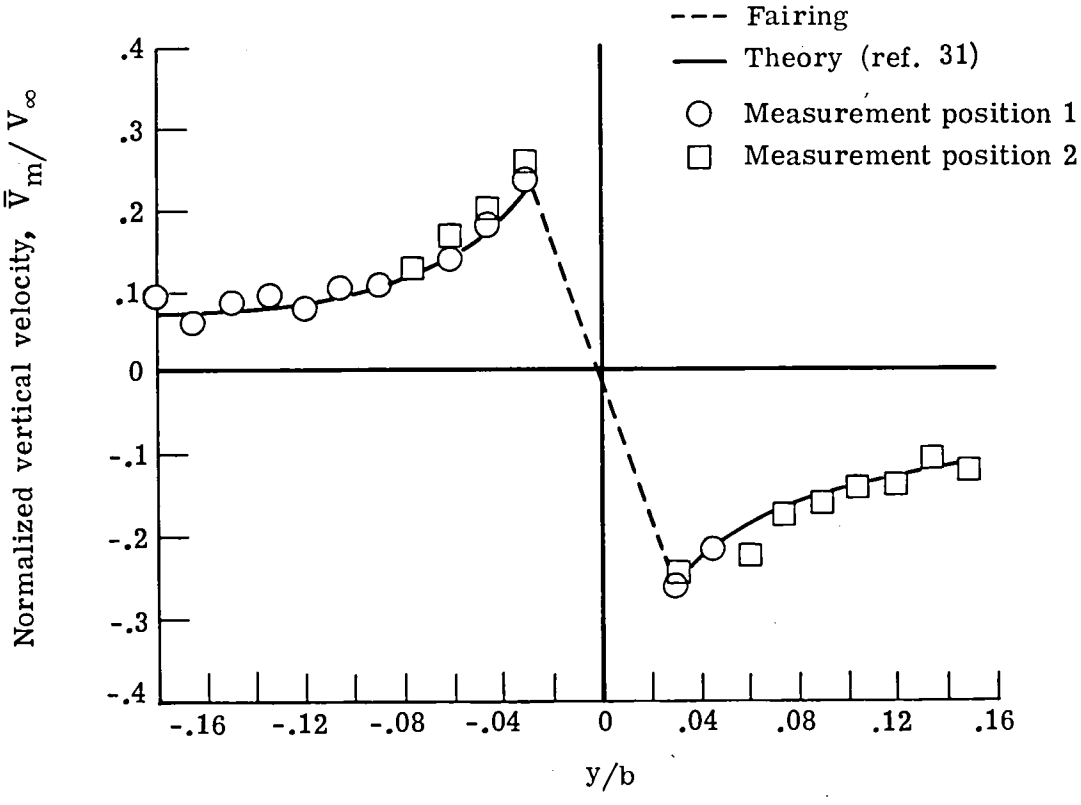

Figure 11.- Vertical velocity distribution at x/b = 55, $\alpha = 4^{\circ}$, $C_L = 1.2$, and $V_\infty = 30.9$ m/sec (landing configuration).

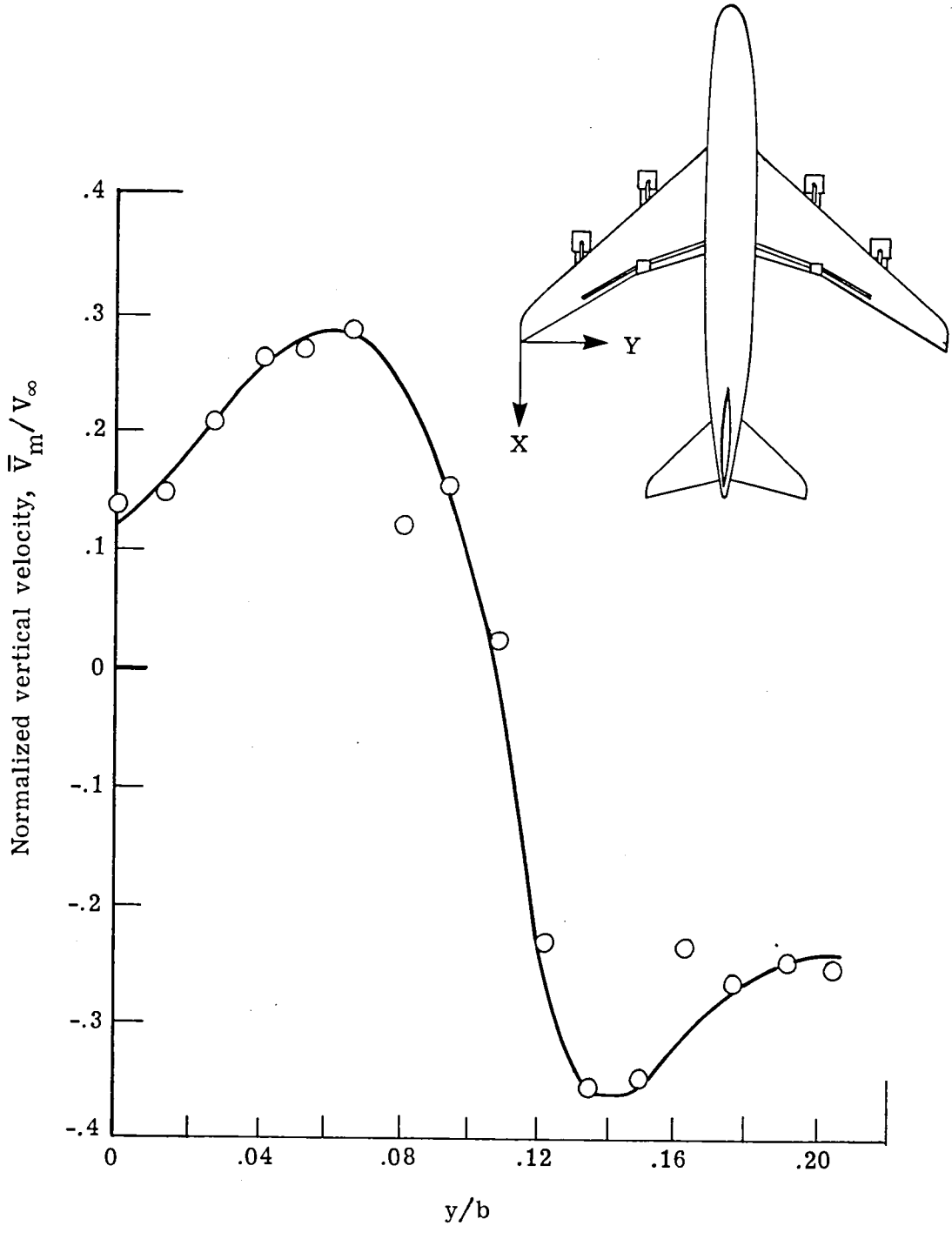

Figure 12.- Vertical velocity distribution at $x/b \approx 1$, $\alpha = 7.7^{o}$, $C_L = 1.4$, and $V_\infty \approx 30$ m/sec (landing configuration).

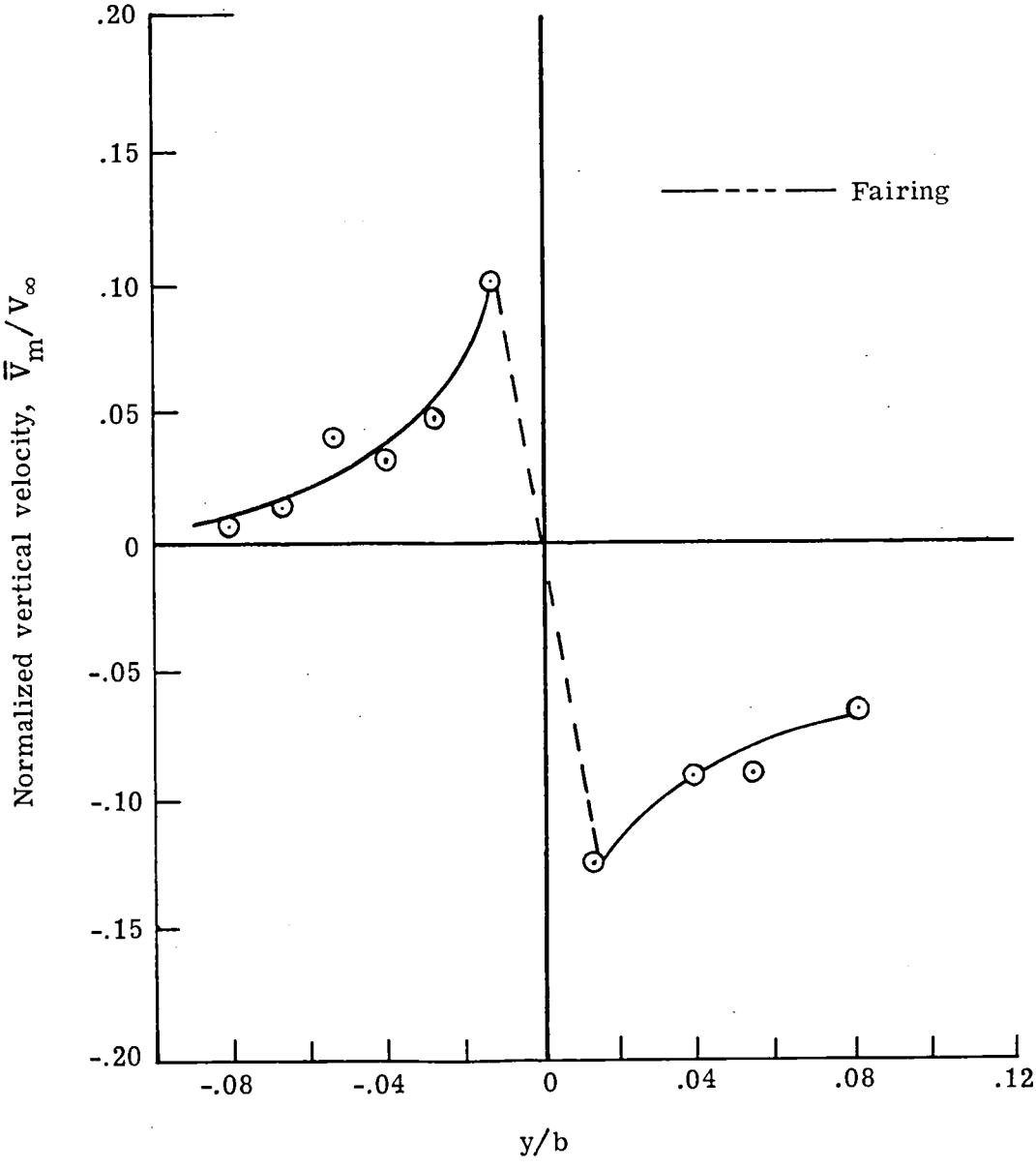

(a) x/b = 7; $\alpha = 6.3^{o}$; $C_L = 0.65$; and $V_\infty \approx 30$ m/sec.

Figure 13.- Vertical velocity distribution in reference to vortex center (cruise configuration).

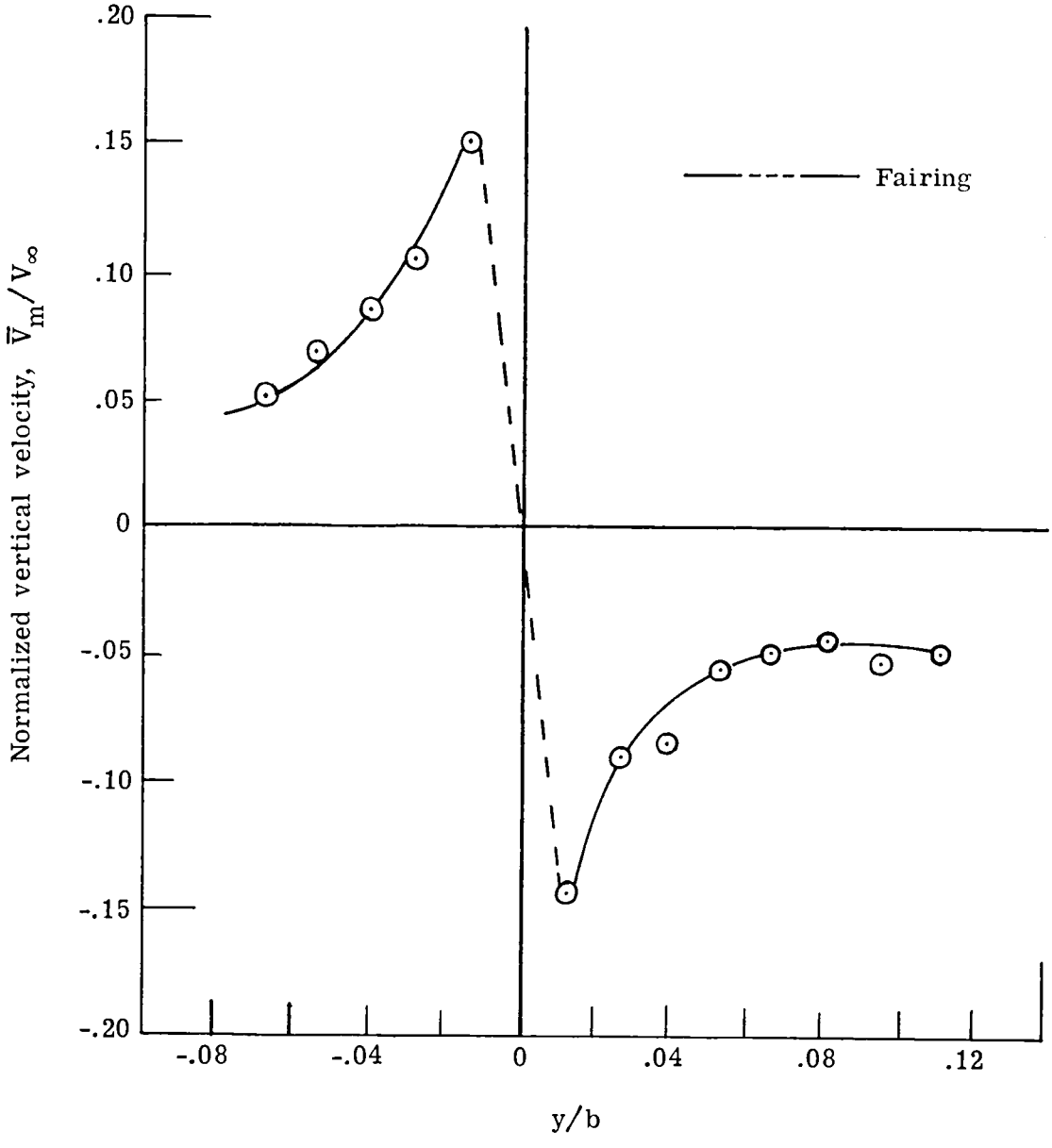

(b) x/b = 16; $\alpha = 6.3^{o}$; $C_L = 0.65$; and $V_\infty \approx 30$ m/sec.

Figure 13.- Continued.

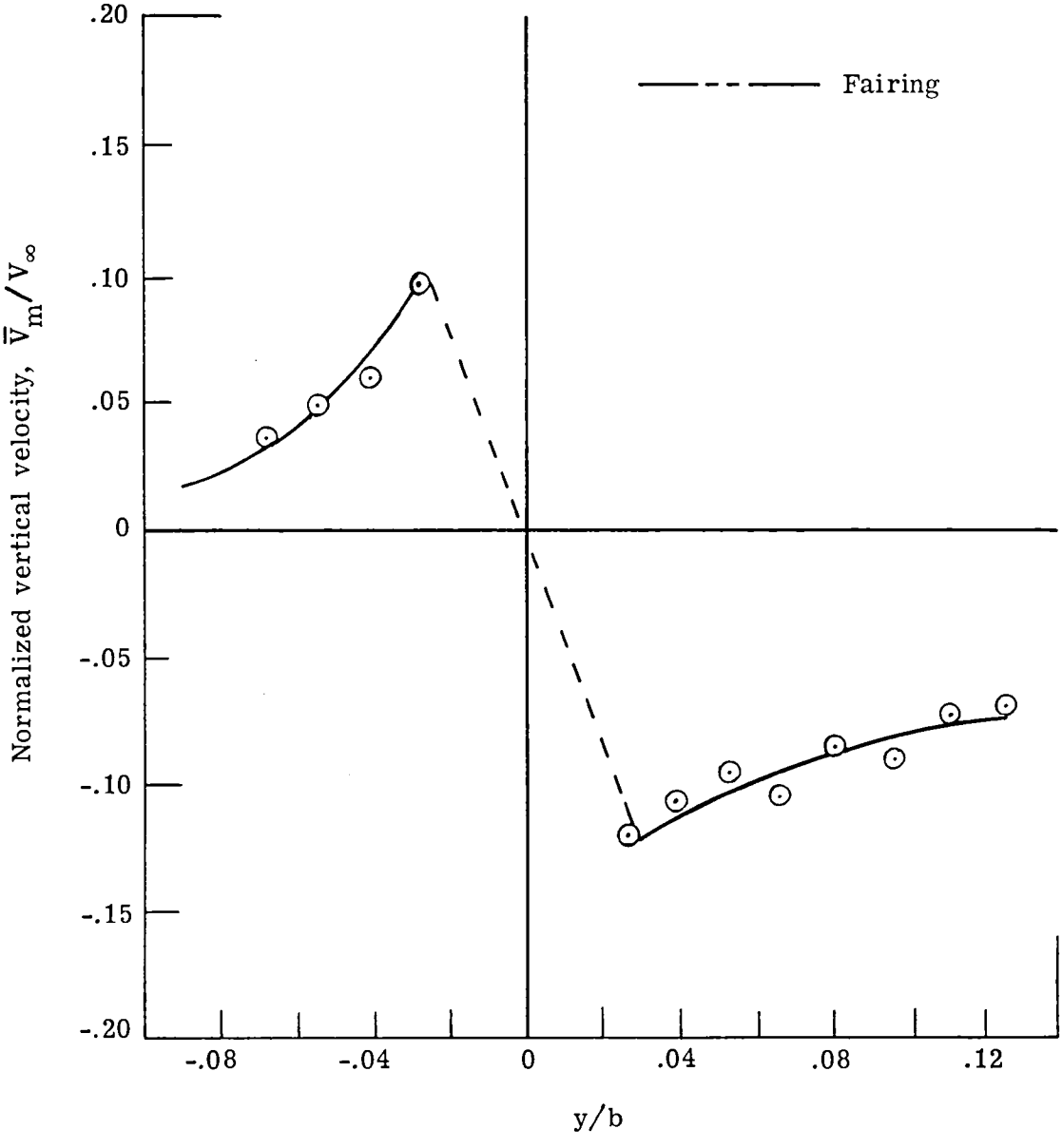

(c) x/b = 32; $\alpha = 6.3^{o}$; $C_L = 0.65$; and $V_\infty \approx 30$ m/sec.

Figure 13.- Concluded.

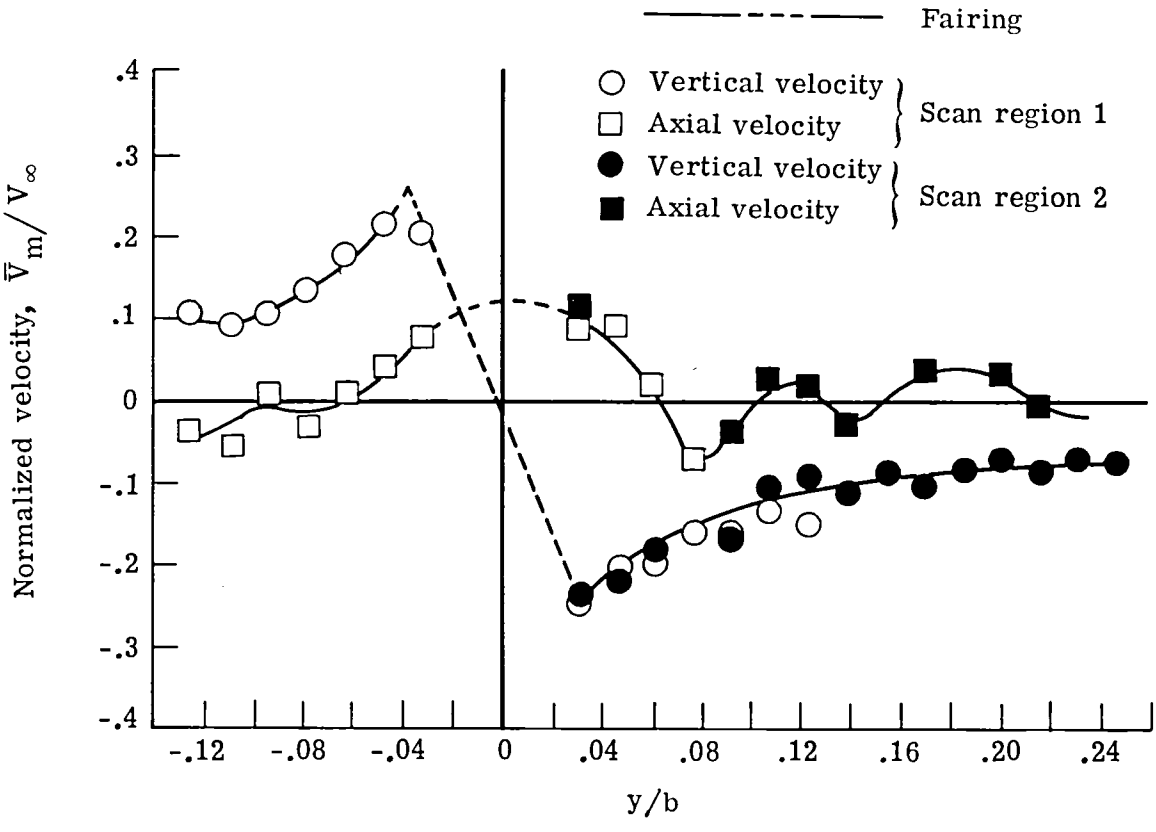

Figure 14.- Vertical and axial velocity distributions in reference to vortex center at $x/b = 30$; $\alpha = 3.5^{o}$; $C_L = 1.2$; and $V_\infty = 30$ m/sec (landing configuration).

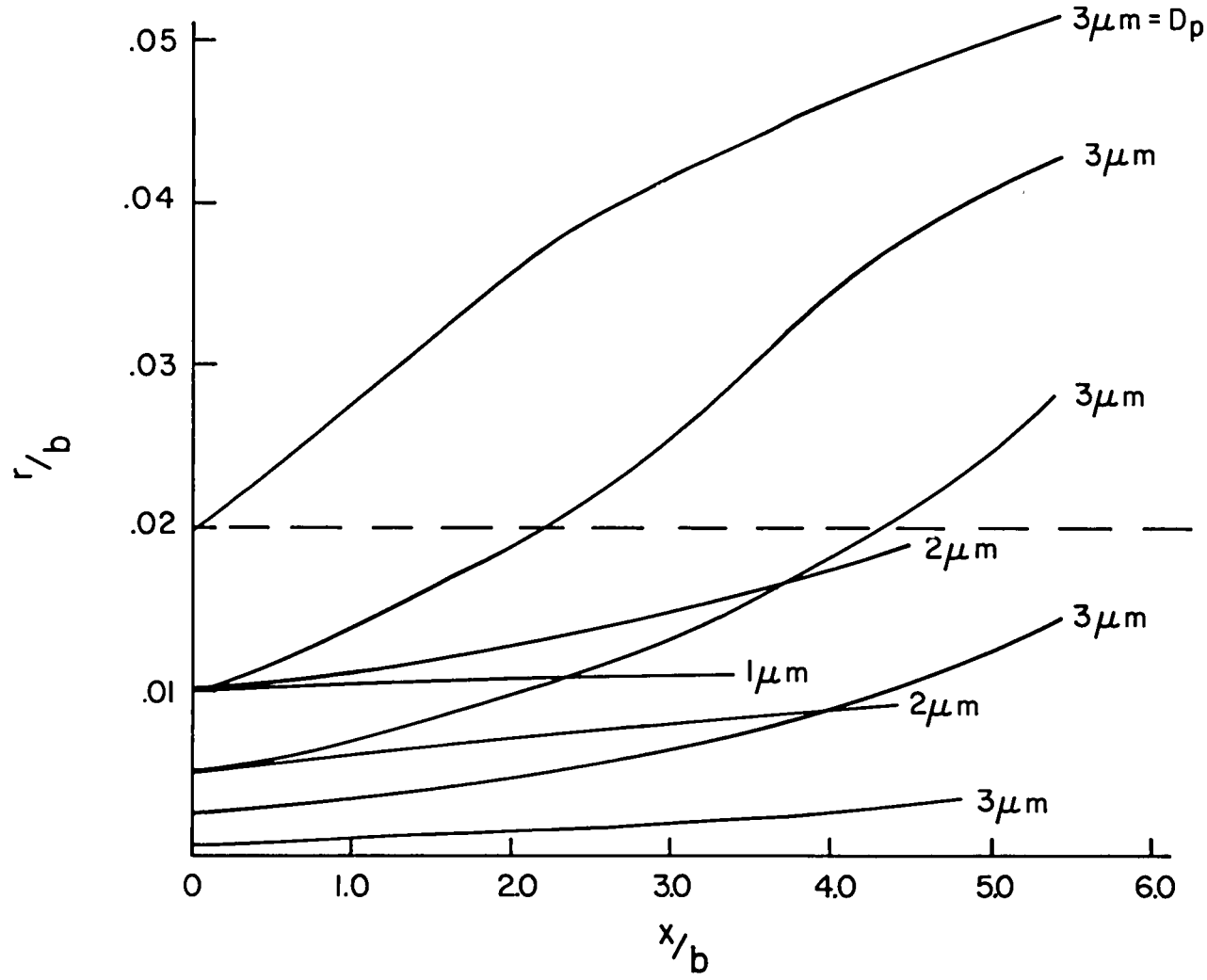

Figure 15.- Radial position for particle passing through vortex.

1. Report No.	2. Government Accession No.	3. Recipient's Catalog No.
NASA TP-1661		

4. Title and Subtitle	5. Report Date
A SCANNING LASER-VELOCIMETER TECHNIQUE FOR MEASURING TWO-DIMENSIONAL WAKE-VORTEX VELOCITY DISTRIBUTIONS	May 1980
	6. Performing Organization Code

7. Author(s)	8. Performing Organization Report No.
Luther R. Gartrell and David B. Rhodes	L-13426
	10. Work Unit No.
	505-31-23-05

9. Performing Organization Name and Address	11. Contract or Grant No.
NASA Langley Research Center Hampton, VA 23665	

12. Sponsoring Agency Name and Address	13. Type of Report and Period Covered
National Aeronautics and Space Administration Washington, DC 20546	Technical Paper
	14. Sponsoring Agency Code

15. Supplementary Notes

Appendix by Michael J. Walsh.

16. Abstract

A rapid scanning two-dimensional laser velocimeter (LV) has been used to measure simultaneously the vortex vertical and axial velocity distributions in the Langley Vortex Research Facility. This system utilized a two-dimensional Bragg cell for removing flow-direction ambiguity by translating the optical frequency for each velocity component, which was separated by band-pass filters. A rotational scan mechanism provided an incremental rapid scan to compensate for the large displacement of the vortex with time. The data were processed with a digital counter and an on-line minicomputer. Vaporized kerosene (0.5-μm to 5-μm particle sizes) was used for flow visualization and LV scattering centers. The overall measured mean-velocity uncertainty is less than 2 percent. These measurements were obtained from ensemble averaging of individual realizations.

17. Key Words (Suggested by Author(s))	18. Distribution Statement
Laser velocimeter Velocity measurements Test techniques Wakes Vortices	Unclassified – Unlimited Subject Category 35

19. Security Classif. (of this report)	20. Security Classif. (of this page)	21. No. of Pages	22. Price*
Unclassified	Unclassified	40	$4.50

*For sale by the National Technical Information Service, Springfield, Virginia 22161

NASA-Langley, 1980